Dynamic response of adhesion complexes: Beyond the single-path picture

Denis Bartolo,[1,*] Imre Derényi,[2,†] and Armand Ajdari[1,‡]
[1]*Laboratoire de Physico-Chimie Théorique, UMR 7083 CNRS, ESPCI, 10 rue Vauquelin, F-75231 Paris Cédex 05, France*
[2]*Institut Curie, UMR 168, 26 rue d'Ulm, F-75248 Paris Cédex 05, France*
(Received 25 June 2001; published 10 May 2002)

We analyze the response of molecular adhesion complexes to increasing pulling forces (dynamic force spectroscopy) when dissociation can occur along either one of two alternative trajectories in the underlying multidimensional energy landscape. A great diversity of behaviors (e.g., nonmonotonicity) is found for the unbinding force and time as a function of the rate at which the pulling force is increased. In particular we identify a class of ''harpoon'' stickers that bind easily but resist strong pulling efficiently. Using existing data, we also demonstrate the consequent difficulty of unambiguously determining the features of the energy landscape from such single-molecule pulling experiments.

DOI: 10.1103/PhysRevE.65.051910 PACS number(s): 87.15.−v, 82.37.−j, 82.20.Kh, 33.15.Fm

INTRODUCTION

The last decades have witnessed a remarkable development of physical investigation methods to probe single molecules or complexes by various micromanipulation means. Techniques have been put forward to probe the unfolding of proteins and to quantify the strength of adhesion structures [1–5]. An important step in this direction is the proposal of the group of Evans *et al.* to use soft structures to pull on adhesion complexes or molecules at various loading rates (dynamic force spectroscopy) [6]. Moving the other end of the soft structure at constant velocity induces on the complex a pulling force that increases linearly in time $f=rt$. Measuring the typical rupture time t_{typ} yields a typical rupture force $f_{\mathrm{typ}}=rt_{\mathrm{typ}}$ that depends on the pulling rate r. This provides information as to the energy landscape of the bound complex. Indeed, in many situations one observes a linear increase of f_{typ} with $\log(r)$, which can be understood within a simple adiabatic Kramers picture for the escape from a well (bound/attached state) over a barrier of height E located at a projected distance x from the well along the pulling direction. The progressive increase of the force results in a corresponding increase of the escape rate, so that, in agreement with some experiments [6], the typical rupture force *increases logarithmically with r*: $f_{\mathrm{typ}}\simeq[k_{\mathrm{B}}T/x]\ln[rx/(k_{\mathrm{B}}T\omega)]$, where ω is the escape rate in the absence of force. The rupture time on the other hand *decreases with r*. The occurrence in some cases of two successive straight lines in a $[f_{\mathrm{typ}},\log(r)]$ plot has been argued to be the consequence of having two successive barriers along the one-dimensional (1D) escape path, the intermediate one showing up in the response at fast pulling rates [6] [Figs. 1(a) and 2]. Other theories have tried to back up more complete information as to the overall effective 1D potential landscape by an analysis of the probability distribution for rupture time and of the statistics of trajectories before rupture [7,8]. Assemblies in series and in parallel of such 1D bonds have also been considered [9–11].

In this paper we point out limitations arising from the *a priori* assumption of a single-path topology of the energy landscape for the interpretation of such experiments. From the analysis of simple examples with a two-path topology, we draw three conclusions: (i) first, the dependence of the rupture force and rupture time on the pulling rate can take various forms, including *nonmonotonic* behavior (see e.g., Figs. 3–5). (ii) Second, the main features of the energy landscape cannot be unambiguously deduced from a $[f_{\mathrm{typ}},\log(r)]$ plot, as very different landscapes can yield similar curves (Fig. 6). (iii) Third, we propose simple ''harpoon'' designs [Figs. 1(c) and 1(d)] for functionally efficient stickers that can bind easily but strongly resist in a range of pulling forces (Fig. 4).

Obviously for real binding/adhesion complexes, there are

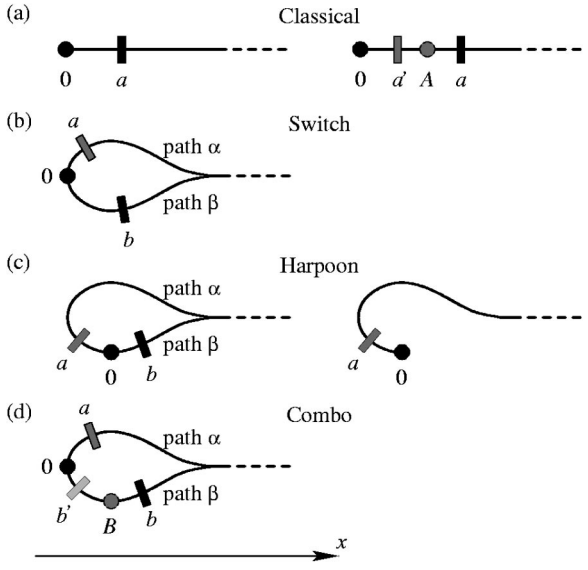

FIG. 1. Sketch of the topology of the main valley of the energy landscape for a few examples. 0 denotes the fundamental bound state, A and B are local minima, and a, a', b, and b' are passes to overcome. To the right (increasing values of x) of the last passes is the continuum that describes unbound states. (a) Classical single-path scheme. (b), (c), and (d) Unbinding can occur through two alternative routes α and β.

*Email address: Denis.Bartolo@espci.fr
†Email address: Imre.Derenyi@curie.fr
‡Email address: armand@turner.pct.espci.fr

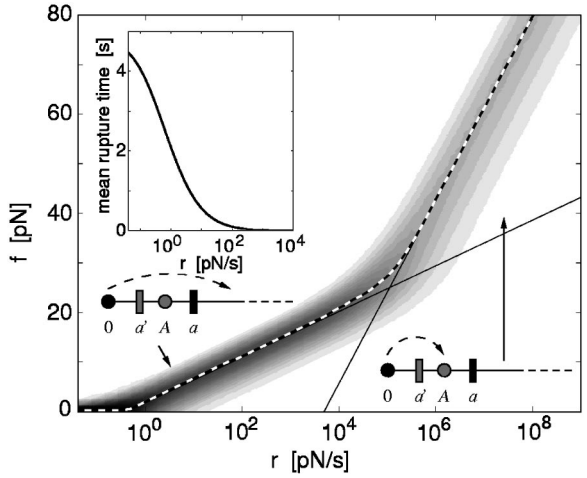

FIG. 2. Classical picture for a single-path energy landscape [6] [Fig. 1(a)]: the probability density $P(f)$ for unbinding at force f is plotted in gray scale as a function of the pulling rate r. The typical force f_{typ} (locus of the maximum of P) is highlighted with a dashed line. Plotted curves correspond to $E_{a'}=12$, $x_{a'}=0.5$, $E_A=9$, $x_A=1$, and $E_a=20$, $x_a=2$. At very low pulling rates unbinding is not affected by the pulling and proceeds over barrier a with a "spontaneous" rate $\omega_0\exp(-E_a)$. For larger pulling rates the typical unbinding force f_{typ} increases linearly with $\log(r)$, with a slope proportional to $1/x_a$. Increasing further the pulling rate leads to a steeper slope $\propto 1/x_{a'}$ corresponding to escape over the inner barrier a'. These asymptotes are depicted with solid lines. The dashed arrows along the drawings indicate which pairs of energy well and barrier are probed in these asymptotic limits. Inset: mean rupture time against pulling rate.

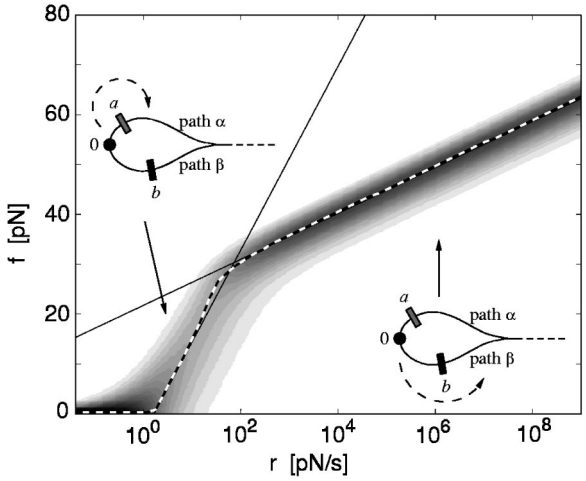

FIG. 3. Switch geometry [Fig. 1(b)]: same quantities as in Fig. 2, for $E_a=20$, $x_a=0.5$, and $E_b=30$, $x_b=2$. Unbinding is controlled by escape over a at low pulling rates, and over b for higher values of r: the slope of the unbinding force (average or typical) decreases from $1/x_a$ to $1/x_b$.

numerous (conformational) degrees of freedom, and the configurational space is clearly multidimensional. This allows for complex energy landscapes and various topologies for the structure of their valleys and passes [12]. Only the probing (pulling) is unidirectional. We note in passing that even for more macroscopic sticky systems, usual adhesion tests for soft adhesives often show up hysteresis loops associated with the existence of more than one degree of freedom [13]. We do not attempt here an exhaustive exploration of effects allowed by the multidimensionality of the phase space, but rather focus on a few simple two-path topologies (Fig. 1), to argue for the three points mentioned above. Their experimental relevance is emphasized by the use of realistic values for the plots throughout and by direct comparison to experimental data in Fig. 6.

MODEL

We consider three simple examples, sketched in Figs. 1(b), 1(c), and 1(d), where detachment can proceed through two alternative routes α and β. A common set of notations can be ascribed for all cases (Fig. 1). From the fundamental bound-state "0," the route α for escape (detachment) is over barriers a, of height E_a located at a projected distance x_a from "0." Alternatively, escape can occur through branch β, over barrier b, of height E_b and projected distance x_b. All energies and projected distances are measured relative to the state "0" (i.e., $E_0=0$ and $x_0=0$). Intermediate barriers a', b', and local minima A and B may exist, with energies $E_{a'}$, $E_{b'}$, E_A, and E_B (all positive), and projected distances $x_{a'}$, $x_{b'}$, x_A, and x_B. In line with typical values from experiments, we choose to write energies in units of $k_BT\simeq 4$ pN nm and distances in nm.

For these quasi-1D-situations, we follow the strategy adopted for single-path geometries [6] and use an adiabatic Kramers theory, an efficient way of obtaining semiquantitatively correct answers [14]. Practically, we describe the time evolution of the probabilities of being in the potential minima (bound states) using transition rates given by Kramers formula for the instantaneous energy profile. We furthermore assume the attempt frequencies to be constant and all equal to ω_0, which sets the time scale in the problem, so that the transition rate from minimum I over the neighboring barrier i is $\omega_0\exp[-(E_i-E_I)+f(t)(x_i-x_I)]$. For the plots of Figs. 2–6 we take arbitrarily $\omega_0=10^8$ s^{-1}. Jump over the rightmost barrier (a or b) of either path corresponds to rupture leading to escape to $x\to\infty$.

We focus on the case where either $E_{b'}$ or E_b is larger than E_a so that α is the "natural" route by which attachment and detachment proceeds *in the absence of pulling*. We also limit ourselves to simple scenarios in which the force is linearly increased in time $f=rt$.

For further reference we recall the classical single-path scenario [Fig. 1(a)] in Fig. 2 for a typical set of parameters, and then we turn to a brief analysis of the three geometries we have introduced [Figs. 1(b), 1(c), and 1(d)].

FIRST CASE: SWITCH

Topology as in Fig. 1(b). Barrier a and b are both located downwards in the pulling direction ($x_a, x_b>0$). The escape proceeds through path α at weak pulling rates as $E_a<E_b$, but if $x_b>x_a$ it switches to path β for pulling forces f large enough such that $E_a-fx_a>E_b-fx_b$. The result (see Fig. 3)

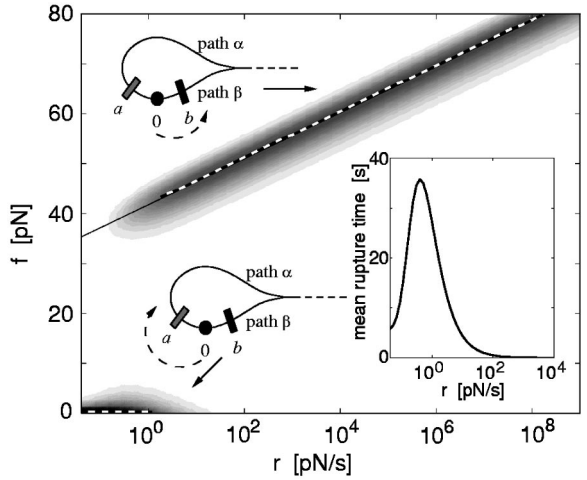

FIG. 4. Harpoon geometry [Fig. 1(c)]: same quantities as in Fig. 2, for $E_a=20$, $x_a=-2$, $E_b=40$, and $x_b=2$. Pulling impedes unbinding through the spontaneous route α, so that for strong enough pulling, escape is controlled by the higher barrier b, resulting in a jump of the typical unbinding force and time. Inset: the average unbinding time is nonmonotonic.

is then a succession of two straight lines of decreasing slopes in the $[f_{\rm typ},\log(r)]$ plot, a feature forbidden in the single-path picture. The first slope ($\propto 1/x_a$) is characteristic of the spontaneous route α while the second ($\propto 1/x_b$) provides information on the alternative route β. Similar curves are expected for the rupture of two bonds in series, which is a particular

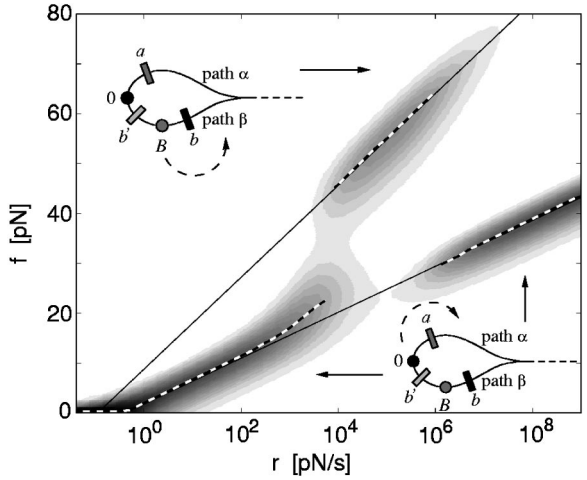

FIG. 5. "Selective harpoon" from the combo topology [Fig. 1(d)]: same quantities as in Fig. 2, for $E_a=20$, $x_a=2$, $E_{b'}=10$, $x_{b'}=0.5$, $E_B=5$, $x_B=1.5$, $E_b=27$, and $x_b=2.5$. At low pulling rates the spontaneous path α is used. Upon increase of r, larger forces are employed and the minimum B becomes favorable as compared to 0. As $E_{b'}$ is not too large, equilibration of population then empties 0 in B, so that escape eventually occurs from B over b, resulting in a higher straight line of slope $\propto 1/(x_b-x_B)$. At even higher pulling rates, because $x_a>x_{b'}$, the escape over a becomes faster than this equilibration, and path α is used again. Barrier a controls the behavior at low and high rates, but in an intermediate window, a stronger bonding is provided by barrier b. The typical (dashed line) or average unbinding force is nonmonotonic.

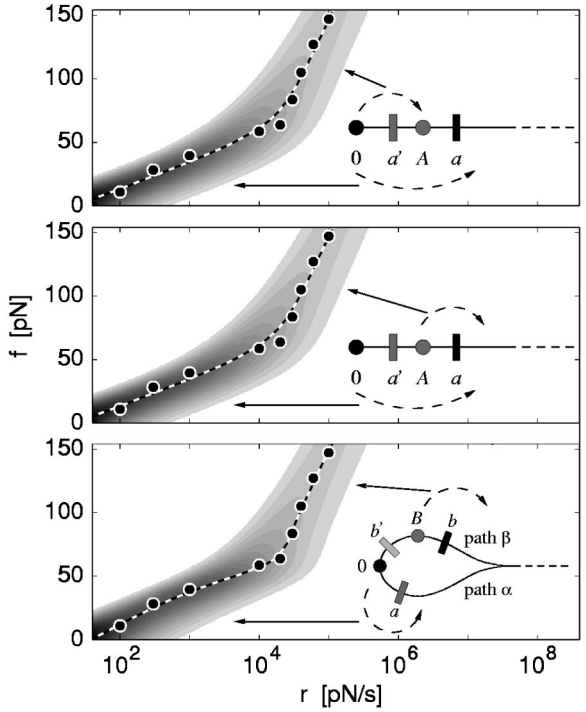

FIG. 6. Experimental data on the L-selectin [17] (circles) and curves from quite diverse energy landscapes that all provide good fits. (a) Classical single path of Fig. 1(a), with the numbers deduced by the authors of [17] from their data: $E_{a'}=13.75$, $x_{a'}=0.08$, $E_A=7.5$, $x_A=0.25$, $E_a=17.5$, and $x_a=0.45$. (b) Classical single path of Fig. 1(a), with $E_{a'}=10$, $x_{a'}=0.2$, $E_A=3.75$, $x_A=0.37$, and $E_a=17.5$, $x_a=0.45$. (c) Combo two-path geometry [Fig. 1(d)], with $E_a=17.3$, $x_a=0.32$, $E_{b'}=13$, $x_{b'}=0.4$, $E_B=7$, $x_B=0.6$, and $E_b=20.8$, $x_b=0.68$. Thanks to the two-path topology, the third scenario is able to account for a slight decrease of the slope at intermediate values.

case of this switch topology [9]. In the trivial case $x_a>x_b$ route β is never explored so that the single-path picture applies.

To clarify the calculation leading to the plot in Fig. 3, we describe the evolution of the probability of attachment $p(t)$ at time t of the system initially attached at time $t=0$ [$p(0)=1$] by

$$\frac{dp}{dt}(t)=-\omega_0(e^{-E_a+f(t)x_a}+e^{-E_b+f(t)x_b})p(t). \qquad (1)$$

Solving Eq. (1) numerically with $f=rt$ yields $p(t)$ and therefore the probability density for the unbinding force $P(f)=-r^{-1}dp/dt$. In the plots, this distribution is suggested through a gray scale, while the location of its maximum which defines the typical value $f_{\rm typ}$, is highlighted with a dashed line. Similar procedures are used for the following examples, with thermal equilibrium between the bound states assumed as initial condition.

SECOND CASE: HARPOON

Topology similar to the previous one but with $x_a<0$ [Fig. 1(c)]. The main feature here is that as the pulling force in-

creases, the probability to escape over a decreases. Therefore the system gets ''stuck'' in route β [15]. If the barrier E_b is infinite [left side of Fig. 1(c)], there is a finite probability $p_\infty = \exp[-\omega_0(r|x_a|)^{-1}e^{-E^a}]$ that unbinding never occurs. For a finite but high barrier E_b, pulling eventually results in unbinding but at high rupture forces (see Fig. 4). The topology thus allows here to form ''easily'' (i.e., over barrier a) a ''harpoon'' sticker that can resist strong pulling. Correspondingly the mean unbinding time increases first with pulling rate (a phenomenology connected to the negative resistance analyzed in Ref. [16]), before decreasing for larger values when activated escape over b dominates. Note that the probability distribution $P(f)$, now consists of two separate ensembles, which coexist over a narrow region of pulling rates. This is in contrast with Fig. 3 where there is a continuous evolution of a single cloud.

THIRD CASE: COMBO

The alternative route consists of two barriers and a local minimum B [Fig. 1(d)], and we focus on the case where $E_{b'}$ is smaller than the two others.

Thanks to the increased complexity and number of parameters in this case many scenarios can occur, covering features already unveiled in Figs. 2–4 (e.g., switch and harpoon). More intricate pictures can also show up, as depicted in Fig. 5. An explanation of this example is given in the caption, illuminating how for low or high pulling rates barrier a controls the behavior, whereas for intermediate values, the secondary and stronger barrier b limits unbinding. Two features are striking. First, the unbinding force (typical or average) is no more monotonic. Second, branch β results in a strengthening of the binding complex for a given window of pulling rates r (selective harpoon).

DISCUSSION

The analysis of the three simple examples above has unveiled a wide range of behaviors that one may expect from dynamic force spectroscopy measurements (see Figs. 3–5). Conversely, we also stress the point (ii) mentioned in the Introduction: even clear-cut outcomes of experiments, such as the succession of two lines of increasing slopes, do not constitute unambiguous signatures of the energy landscapes. To substantiate this, experimental data on the L-selectin from [17] are plotted against calculations corresponding to sensibly different landscapes in Fig. 6. Not only are the typical and average unbinding forces very similar in the three cases, but so are the probability distributions for most values of r, so that it is difficult to discriminate between the three landscapes from this sole set of data. This would require additional information, that could, e.g., be obtained using other temporal sequences than the simple $f=rt$.

Eventually we point out that the harpoon geometries proposed here constitute a very obvious paradigm for efficient stickers. Attachment of the sticker can proceed through route α with a possibly not too high barrier E_a. The harpoon configuration then allows us to benefit from the much stronger b barrier for a given window of pulling forces, making the sticker more efficient in these conditions. This ''hook'' design is obviously a favorable strategy for adhesion complexes, the function of which is to maintain adhesion under the action of well-defined tearing stresses. It would be surprising if advantage was not taken of this by some biological systems.

[1] M. Rief, M. Gautel, F. Oesterhelt, J.M. Fernandez, and H.E. Gaub, Science **276**, 1109 (1997); M.S. Kellermayer, S.B. Smith, H.L. Granzier, and C. Bustamante, *ibid.* **276**, 1112 (1997).

[2] M.G. Poirier, A. Nemani, P. Gupta, S. Eroglu, and J.F. Marko, Phys. Rev. Lett. **86**, 360 (2001).

[3] D.A. Simson, M. Strigl, M. Hohenadl, and R. Merkel, Phys. Rev. Lett. **83**, 652 (1999).

[4] T. Nishizaka, R. Seo, H. Tadakuma, K. Kinosita, and S. Ishiwata, Biophys. J. **79**, 962 (2000).

[5] A. Pierre, A.M. Benoliel, P. Bongrand, and P.A. van der Merwe, Proc. Natl. Acad. Sci. U.S.A. **93**, 15 114 (1996).

[6] E. Evans and K. Ritchie, Biophys. J. **72**, 1541 (1997); R. Merkel, P. Nassoy, A. Leung, K. Ritchie, and E. Evans, Nature (London) **397**, 50 (1999).

[7] G. Hummer and A. Szabo, Proc. Natl. Acad. Sci. U.S.A. **98**, 3658 (2001).

[8] B. Heymann and H. Grubmüller, Phys. Rev. Lett. **84**, 6126 (2000).

[9] E. Evans, Faraday Discuss. **111**, 1 (1998); E. Evans, Annu. Rev. Biophys. Biomol. Struct. **30**, 105 (2001).

[10] U. Seifert, Phys. Rev. Lett. **84**, 2750 (2000).

[11] M. Rief, J.M. Fernandez, and H.E. Gaub, Phys. Rev. Lett. **81**, 4764 (1998).

[12] E. Paci and M. Karplus, Proc. Natl. Acad. Sci. U.S.A. **97**, 6521 (2000).

[13] K.L. Johnson, K. Kendall, and A.D. Roberts, Proc. R Soc. London, Ser. A **324**, 301 (1971).

[14] J. Shillcock and U. Seifert, Phys. Rev. E **57**, 7301 (1998).

[15] This behavior is closely related to the ''catch bonds'' alluded to in: M. Dembo, D. C. Torney, K. Saxman, and D. Hammer, Proc. R. Soc. Lond. **234**, 55 (1988).

[16] G.A. Cecchi and M.O. Magnasco, Phys. Rev. Lett. **76**, 1968 (1996).

[17] E. Evans, A. Leung, D. Hammer, and S. Simon, Proc. Natl. Acad. Sci. U.S.A. **98**, 3784 (2001); data on L-selectin with PSGL-1 ligand from Fig. 3(a).